CHANDRA OBSERVATIONS OF RELATIVISTIC AGN JETS

Daniel A. Schwartz,[1]

RESUMEN

El resumen será traducido al español por los editores. This article reviews Chandra survey observations of jets in quasars. We interpret the X-ray emission in terms of inverse Compton scattering on the Cosmic Microwave Background. Both the spectral energy distribution and X-ray/radio morphologies support such a supposition, in many cases. This requires bulk relativistic motion of the jets at distances of 100's of kpc from the quasar, and allows estimates of the rest frame magnetic fields; provided we assume minimum energy conditions. The kinetic flux carried by the jets is very large and transported efficiently. Such jets in clusters would carry more than enough energy to balance cooling flows. The IC/CMB mechanism implies that jets should maintain a constant surface brightness to arbitrarily large redshifts – no specific evidence exists yet to support this expectation.

ABSTRACT

This article reviews Chandra survey observations of jets in quasars. We interpret the X-ray emission in terms of inverse Compton scattering on the Cosmic Microwave Background. Both the spectral energy distribution and X-ray/radio morphologies support such a supposition, in many cases. This requires bulk relativistic motion of the jets at distances of 100's of kpc from the quasar, and allows estimates of the rest frame magnetic fields; provided we assume minimum energy conditions. The kinetic flux carried by the jets is very large and transported efficiently. Such jets in clusters would carry more than enough energy to balance cooling flows. The IC/CMB mechanism implies that jets should maintain a constant surface brightness to arbitrarily large redshifts – no specific evidence exists yet to support this expectation.

Key Words: **X-RAYS: GALAXIES — GALAXIES: JETS — QUASARS: GENERAL — COSMIC MICROWAVE BACKGROUND**

1. INTRODUCTION

Jets have been of key interest in radio astronomy for decades. They carry the very large quantities of energy which are observed in radio lobes at distances up to Mpc from the active galaxy engine (Begelman, Blandford, & Rees 1984). This large energy flux may be a non-negligible, and in some cases a dominant, component of the black hole energy generation budget. Jets from active galactic nuclei (AGN) in clusters of galaxies are inferred to provide energy to stop the cooling flows which are commonly observed (Fabian 1994).

The results of 25 years of radio observations of jets in AGN have provided much information, and raised several issues which remain to be answered. They have revealed that the jets are relativistic, the theme topic of this conference, by observing apparent superluminal motions on pc-scales and by observations that pc to kpc scale jets are typically one-sided. The latter is explained by Doppler boosting of the jet propagating toward us, and diminution of the jet propagating away from our line of sight. We know that the radio and optical emission are due to synchrotron radiation from observation of polarization. We still need to learn whether the positively charged component of the jets are positrons or protons, how the relativistic electrons (and we will include positrons in the term "electrons") are accelerated, and how the jet itself is collimated and accelerated to bulk relativistic motions.

1.1. *X-ray Observations of Jets*

How does X-ray data help to address these questions? By observing the spectral energy distribution (SED) from radio to X-rays we can elucidate the radiation mechanism of the electrons. In turn, this allows independent data to confront the standard synchrotron minimum energy calculations. Under the hypothesis of inverse Compton (IC) scattering on the cosmic microwave background (CMB), which we will discuss in section 2.2, this allows an estimate of the bulk Doppler factor of the jet, and in turn a direct calculation of the kinetic energy flux. Because the energies of the particles radiating into radio, optical, or X-ray bands are quite different, their rate of

[1] Smithsonian Astrophysical Observatory, Cambridge, MA, USA.

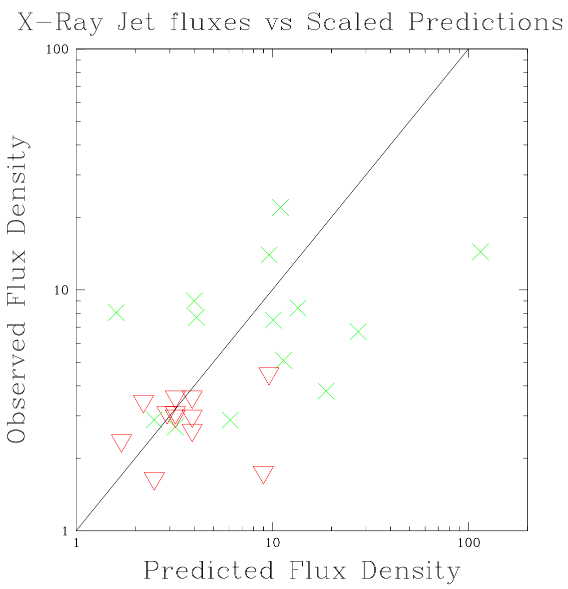

Fig. 1. X-ray jet detections (crosses) and upper limits (down-triangles) for 26 of the first *Chandra* observations in the survey by Marshall et al. (2005). The solid line represents an observed 1 keV X-ray to 5 GHz radio flux density ratio equal to that of PKS 0637-752, which is the basis of the predicted flux density.

energy loss and therefore their lifetimes change with the observed band. If the X-rays arise from synchrotron emission they would give us a window into the extremely high energy electrons, with $\gamma \approx 10^7$, while if they arise from the IC/CMB process their source is the otherwise unobservable electrons with γ= 100 to 1000.

It is only with the sub-arcsecond angular resolution of the *Chandra* X-ray Observatory that the study of jets has become an important topic of X-ray astronomy. Much of this paper will be based on a survey for X-ray emission being carried out by Marshall et al. (2005). The survey was designed following the serendipitous discovery of a powerful X-ray jet in the quasar PKS 0637-752, which was being used as a target for the initial focusing of the *Chandra* telescope (Schwartz et al. 2000). At that time we had no good predictions for what radio jets would have accompanying X-ray emission. We planned short observations, 5 ks, of large numbers of objects in order to establish some predictive criteria and to find X-ray jets which would merit further detailed followup study. We looked at radio maps which had better than 2″resolution, and for which the jet was greater than 2″ in extent. We selected objects which would be detectable in 5 ks, if their ratio of X-ray to radio emission was as large as observed in PKS 0637-752. The parent objects were from two samples of flat spectrum quasars (Murphy, Browne, & Perley 1993; Lovell 1997), which biases the sample toward relativistically beamed objects.

Figure 1 shows the resulting detections (crosses) and upper limits (triangles) for some of the first objects observed. The solid line of equal observed and predicted flux density is the number scaled from PKS 0637-752. Key conclusions from this figure are that we see a distribution in the observed ratio of X-ray to radio jet emission, that PKS 0637-752 may have a higher X-ray flux than average, and that the upper limits to the objects not detected still allow them to be part of the same population distribution. To date, 22 of 37 sources observed have detected X-ray jets. A complementary survey by Sambruna et al. (2002) has detected X-ray jets at a similar rate of about 60%. That survey included Hubble Space Telescope (*HST*) observations of most objects, which allowed a critical evaluation of the emission mechanism in terms of IC/CMB.

1.2. *Outline of This Paper*

In Section 2 we will discuss the X-ray emission mechanism. We present data on the broad band spectral energy distributions, and present the hypothesis that the X-rays arise from inverse Compton scattering on the cosmic microwave background. We review the X-ray jet morphologies in Section 3, and in particular the ratio of X-ray to radio flux density along the length of the jets. In Section 4 we derive magnetic fields, Doppler factors, and kinetic flux of the jets under the IC/CMB hypothesis. The IC/CMB mechanism predicts that the same jets seen locally will maintain their surface brightness to large redshift. Jets at large redshift are discussed in Section 5. We give a brief summary in Section 6.

2. THE X-RAY EMISSION MECHANISM

Radio and optical emission from jets are well established to be synchrotron radiation due to the observation of polarization. Synchrotron emission must be considered in general for the X-ray emission, as it is inferred to occur in Cen A (Schreier, Burns, & Feigelson 1981), the innermost M87 knots (Harris et al. 2003), and many FR I type jets (Worrall, Birkinshaw, & Hardcastle 2001). Thermal bremsstrahlung can be ruled out due to the X-ray spectral shape, the large gas mass which would be required, and at least for PKS 0637-752 from the rotation measure upper limit (Schwartz et al. 2000). The remaining candidate mechanism involves inverse Compton scattering, where the target photons might be from syn-

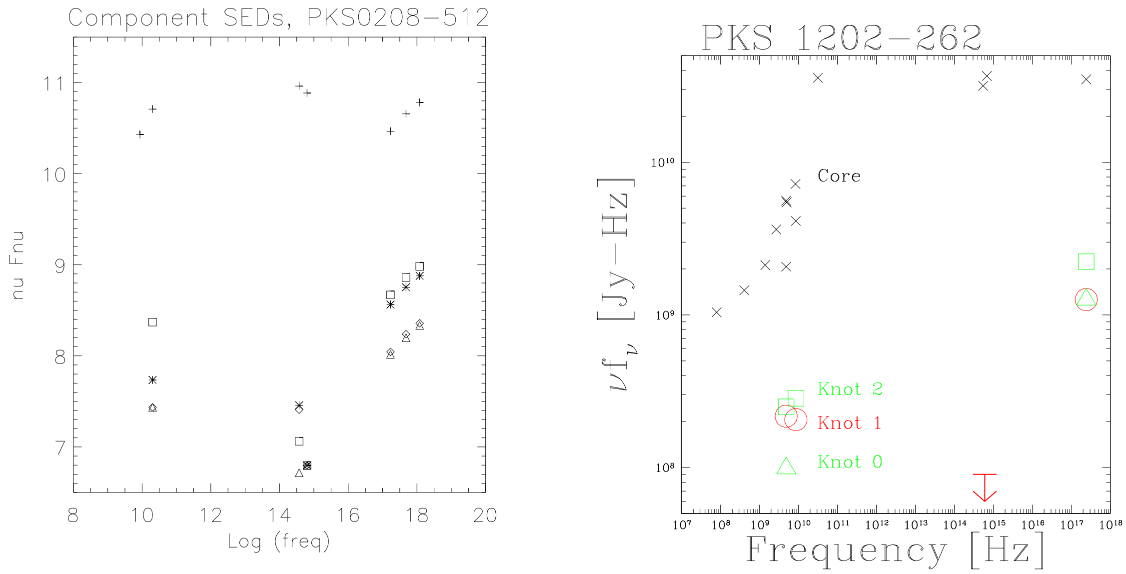

Fig. 2. Broad band spectral energy distribution of two representative X-ray jets observed in the survey by Marshall et al. (2005). The top traces (plus signs and crosses) show νf_ν (or its log) for the quasar core. Bottom symbols give the SED for various regions within the jet. The optical flux densities and upper limit show that the X-ray emission is not a simple extension of the radio synchrotron spectrum.

chrotron self-Compton, from the quasar, or from the cosmic microwave background.

2.1. *Spectral energy distribution*

Figure 2 shows the broad band SED for two quasars, and for spatially distinct regions in their jets. *HST* measurements of PKS 0208-512 (Perlman et al. 2004) and Magellan data for PKS 1202-262 show that the radio synchrotron spectrum cannot simply be extended to produce the X-ray emission. This conclusion remains true even if we consider a spectral break due to energy losses of the highest energy electrons. This leads to the inverse Compton scattering as being the next simplest explanation for the X-ray emission, although models have been formulated to retain a synchrotron origin of the X-rays (). As had been found for PKS 0637-752, (Schwartz et al. 2000), the jet regions are not sufficiently compact to give significant X-ray emission via synchrotron self-Compton. Furthermore, they are too far from the quasar for photons emitted from the core to be the dominant target for IC scattering.

Figure 3 shows the SED for four sources from the survey of Sambruna et al. (2002). They use *Chandra* and *HST* data to detect the X-ray and optical emission, respectively, for two knots in each of their jets. Seven of these eight regions, knot A of 1135-135 being the exception, do not allow simple extrapolation of the radio synchrotron spectrum to the X-ray region. The heavy solid lines show fits to a model

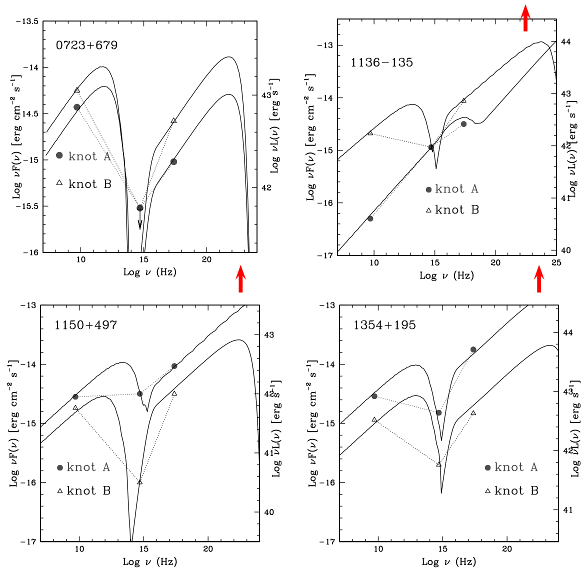

Fig. 3. SED for four X-ray jets taken from Sambruna et al. (2002). Solid lines model the emission as synchrotron radiation in the radio band, with the high energy tail of electrons producing optical synchrotron and a low energy extension of the electrons producing X-rays via IC/CMB.

where synchrotron radiation provides the radio and optical emission, while the X-rays are from IC emission from electrons which are an extrapolation to lower energies of those electrons emitting radio syn-

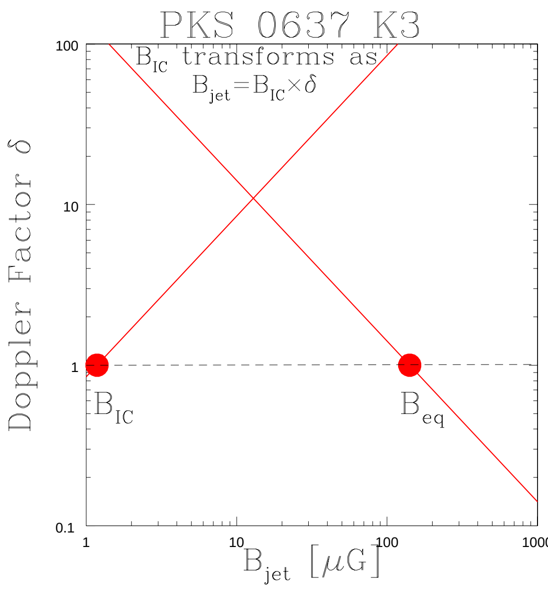

Fig. 4. The dashed horizontal line assumes a non-relativistic jet, with δ=1. In this case the magnetic field calculated assuming equipartition, (the solid dot marked B_{eq}), and the field calculated assuming the X-rays arise from IC/CMB, (the solid dot marked B_{IC}), are inconsistent by a factor of ≈100. However, the solid lines through each dot show how each calculation depends on δ, and their intersection gives a solution with B=15 μG and δ=11, for a region of the jet ≈ 8″ from the quasar PKS 0637-752.

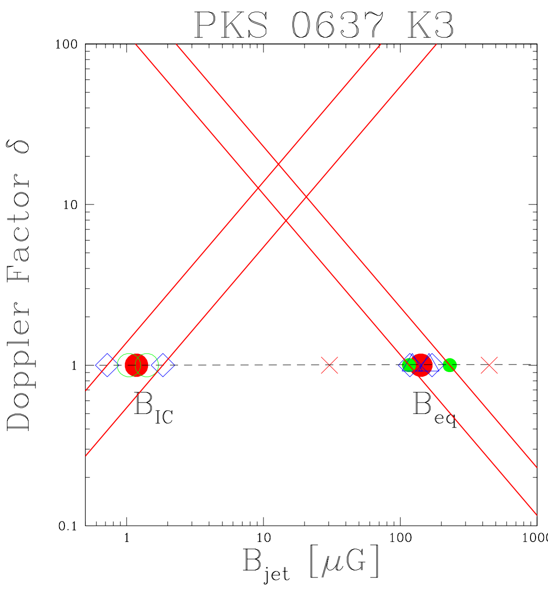

Fig. 5. Estimate of the uncertainty of the calculation shown in Fig. 4. The estimated values of B and δ are dominated by the assumptions made in the minimum energy and IC/CMB models of the source emission (see text). These allow a range of about a factor of 2 in either one of the parameters. Note that the uncertainty is highly correlated for B and δ.

chrotron.

A prediction of the IC/CMB model is that the X-radiation will extend up to the gamma ray region, around 10^{23}Hz. With the uncertainties in the spectral slope of the X-rays, three of the sources might be detectable by the *GLAST* mission, for which the approximate sensitivity for a two year survey is shown by the thick up-arrows.

2.2. *Inverse Compton scattering on the Cosmic Microwave background*

When Schwartz et al. (2000) attempted to explain the X-ray emission from the jet in PKS 0637-752 they realized that with the magnetic field strength calculated via minimum energy or near equipartition arguments (Moffet 1975), the corresponding density of relativistic electrons was far too low to give the measured X-ray flux. In fact they gave no satisfactory explanation, listing gross departure from equipartition, inhomogeneous synchrotron or an unlikely coincidence of a jet which was Doppler diminished in our direction as possibilities. Tavecchio et al. (2000) and Celotti et al. (2001) resolved this dilemma by noting the result of Dermer and Schlickeiser (1994) that the energy density of the CMB is enhanced by a factor Γ^2 in the rest frame of a relativistic jet moving with bulk Lorentz factor Γ.

Figure 4 illustrates this calculation for one of the regions in the jet of PKS 0637-752. We use the formalism of Felten & Morrison (1966) to calculate the magnetic field for which a single electron spectrum of the form $n(\gamma)=n_0\,\gamma^{-m}$ electrons cm^{-3} per unit γ, would produce the radio emission via synchrotron radiation and the X-ray emission via IC/CMB. If we assume non-relativistic motion of the jet then the Doppler factor $\delta=[\Gamma(1-\beta\cos(\theta))]^{-1}$ is unity, indicated by the dashed line. In that case the magnetic field would be as shown by the large solid dot marked B_{IC}. Similarly, the magnetic field calculated by assuming the synchrotron emission is produced by electrons radiating in a magnetic field under conditions of minimum energy would be given by the large solid dot marked B_{eq}. The factor of ≈ 100 difference in these two magnetic field values is resolved by considering the relativistic motion of the jet with respect to the CMB. In that case, the value of the minimum energy magnetic field in the jet rest frame, B_{jet} $=B_{eq}/\delta$ while the value of the jet frame field which produces the observed ratio of radio synchrotron to IC/CMB X-rays is given by $B_{jet} = B_{IC} \times \delta$. These

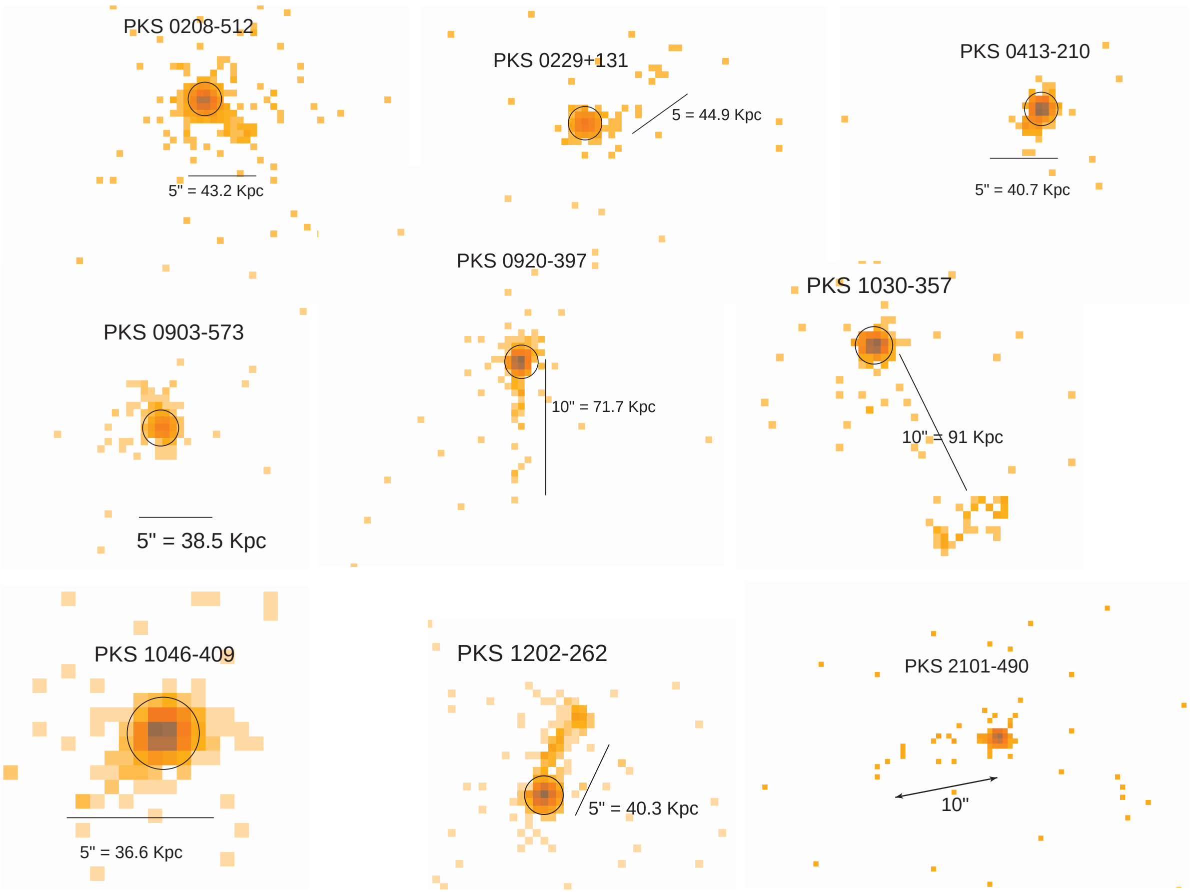

Fig. 6. X-ray images of 9 of the first 20 jet observations by Marshall et al. (2005). X-rays between 0.5 and 7 keV are sorted into bins of 4.″92, with the faintest level being one count. Background is of the order of 0.003 counts per bin.

two equations give a solution for the values of B_{jet} and δ, shown in Figure 4 as the intersection of the two diagonal lines at B=14.8μG and δ=11.2.

The uncertainty in those values is dominated by the assumptions made in the model of near-equipartition synchrotron and IC/CMB emission. Figure 5 shows a range of values of B and δ which might result for the region shown in Figure 4. The greatest uncertainty is the assumption of minimum energy. The energy density U increases $\propto B^{-3/2}$ for smaller magnetic fields, and increases $\propto B^2$ for larger fields. For energy 10 times the minimum, the crosses left and right of B_{eq} in Figure 5 give the resulting fields. In applying the minimum energy synchrotron formalism, e.g., from Moffet (1975), we must assume values of the radio spectral index, the lower and upper frequency cutoff of the observed radio spectrum, the volume filling factor, and the ratio, k, of proton to electron energy density, none of which are directly observed. We have assumed an energy spectral index α=0.7, a radio spectrum range $\nu_1=10^6$ Hz to $\nu_2=10^{12}$ Hz, and unity for the volume filling factor and for the ratio of proton to electron energy density. The open diamonds give the results for a spectral index of 0.6 or 0.8, and the open triangles for $\nu_1 = 10^5$ or 10^7. We adopt an uncertainty region corresponding to the smaller solid dots, which show the field calculated for values of k=0 or k=10.

For the magnetic field calculated from IC/CMB considerations, the spectral index error dominates the uncertainty. We show the change due to the Poisson errors in the numbers of X-ray counts by the open circles. We can then estimate a range of about a factor of two in which B or δ might fall: B= 9 to 21 μGauss and δ = 7.7 to 18. Note that these two parameters are highly correlated, so one cannot independently assign each to the extreme value. Since we cannot quantify the probability of the error in our model assumptions, we cannot assign a numerical confidence to this overall uncertainty. Schwartz et al. (2006) give a more detailed discussion of these uncertainties as applied to several sources in the sur-

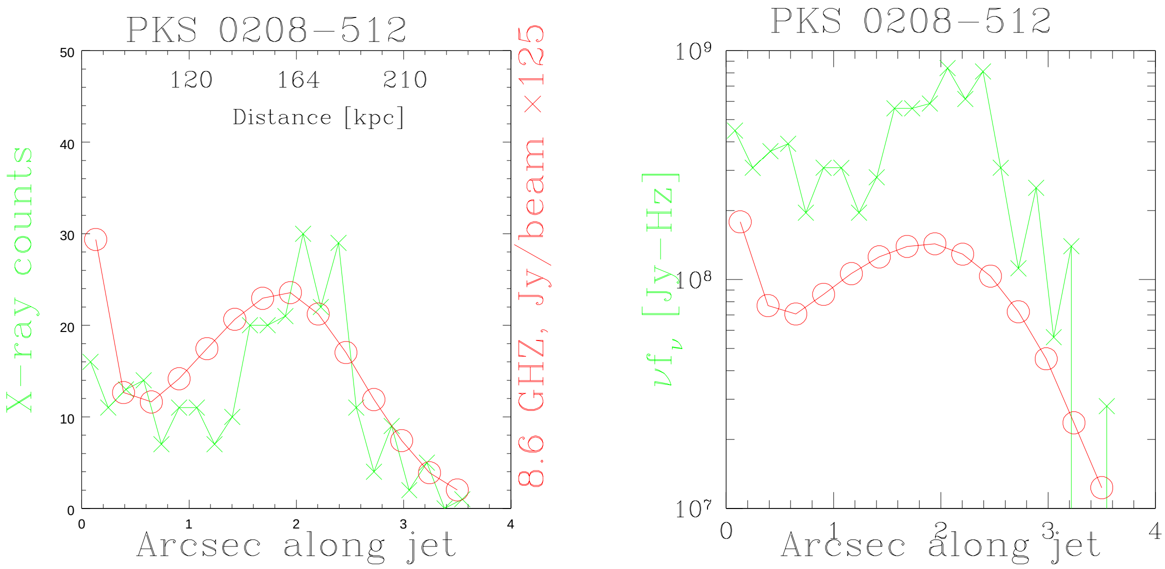

Fig. 7. Comparison of the X-ray and radio profiles for the jet of PKS 0208-512. In the left panel, crosses are X-ray counts per bin, and circles are 8.64 GHz flux density in Jy per beam multiplied by 125 to better compare with the X-rays. Distance along the jet is measured from a point about $2''$ away from the quasar. Right panel plots νf_ν for both bands in Jy-Hz, showing that the X-rays dominate the energy radiated by the jet.

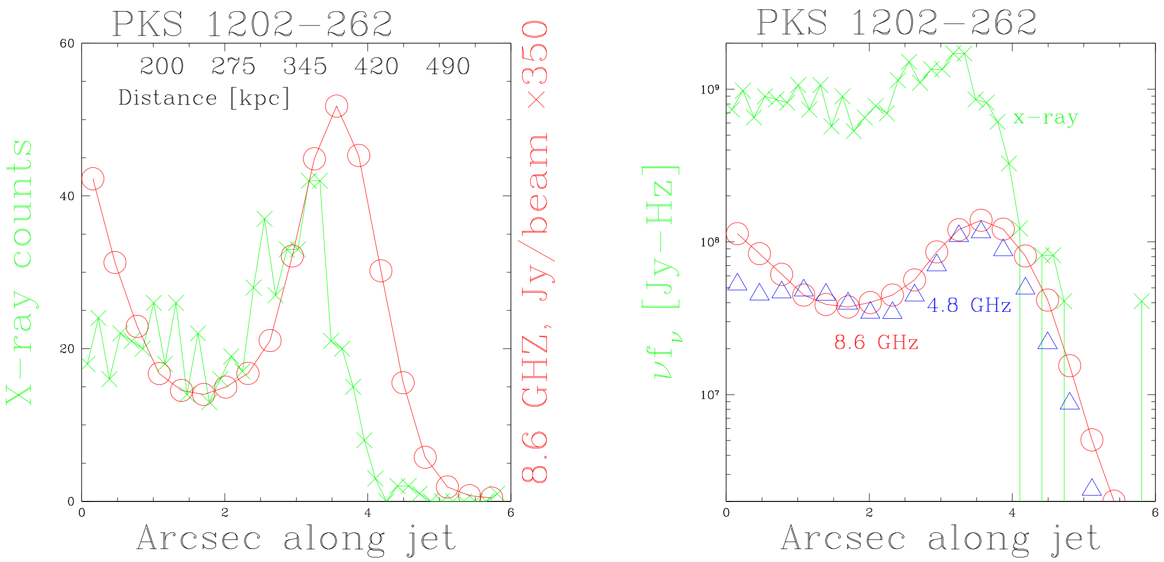

Fig. 8. Comparison of the X-ray and radio profiles for the jet of PKS 1202-262. In the left panel, crosses are X-ray counts per bin, and circles are 8.64 GHz flux density in Jy per beam multiplied by 350. Distance along the jet is measured from a point about $2''$ away from the quasar. Right panel plots νf_ν in Jy-Hz for X-rays (crosses) 8.65 GHz (circles) and 4.8 GHz (triangles), showing that the X-rays dominate the energy radiated by the jet.

vey of Marshall et al. (2005).

3. X-RAY JET MORPHOLOGY

Figure 6 shows X-ray images of nine of the jets detected in our initial set of 5 ks observations (Marshall et al. 2005). The X-ray jet emission is spatially coincident with radio jet emission, and images of the two correlate well although not perfectly. Some of the jets appear to be continuous in X-rays; for example, PKS 0208-512, PKS 1202-262, and the first $4''$ of PKS 0920-397. However, the 5 ks duration of these observations gives a very limited contrast sensitivity, and the "knotty" appearance in objects such as PKS 0229+131, PKS 1030-357 and PKS 2101-490 are based on just a few counts, and need not represent contrast ratios greater than 2. PKS 0920-397 is a case where the X-rays diminish with distance away from the quasar, while the radio jet brightens, similar to the behavior of 3C 273 citepMarshall01. The scale bars of 5″ or 10″ length on each image are labeled with the corresponding distance in the plane of the sky, at the redshift of the object. Since we will deduce Doppler factors of 3 to 12 for these objects, they must be no more than 5° to 20° from our line of sight, so their intrinsic lengths are 3 to 10 times longer than the projections.

Figures 7 and 8 compare the X-ray and radio profiles along two of the jets. In the left hand panels, the crosses plot the number of X-ray counts, and the circles the 8.64 GHz flux density in Jy per beam with an arbitrary scaling so as to more closely overlay the X-ray profile. The projections cover the identical region of space, summing the flux in bins which are 2″ perpendicular to the jet, and with the zero point of distance starting about 2″ from the core to avoid scattered flux from the quasar. The ratio of X-ray to radio flux does not vary by more than a factor of 2 for a length of at least 3.″5 along each jet. Considering the maximum angles for the jets from our line of sight (discussed in Section 4) these correspond to physical lengths of about 250 kpc and 350 kpc for PKS 0208-512 and PKS 1202-262, respectively.

The near constant ratio is quite difficult to understand. To produce the X-rays via synchrotron radiation would require electron Lorentz factors $\gamma \approx 10^7$. The short lifetimes of such electrons, compared to electrons of $\gamma \approx 10^{3-4}$ emitting in the GHz band, requires a quasi-continuous acceleration of electrons to TeV energies. In case that the X-ray emission is IC/CMB, they arise from lower energy, longer lived electrons with $\gamma = 10^{2-3}$. This gives much more flexibility for constructing a near-constant X-ray to radio emission ratio, but carries the extra *ad hoc* assumption that the magnetic field strength remains relatively constant. Understanding the profiles will require self-consistent modeling of the entire length of the jet, including acceleration and transport of the relativistic particles. Conversely, the X-ray profiles provide critical data to test models of jets built to match the radio morphology.

We observe similarly constant X-ray to radio flux ratio over long distances in PKS 0637-752 (Schwartz et al. 2001), and in 1354+19, as shown in Figure 9. The X-ray counting statistics are relatively larger in the latter source, but may indicate a relatively constant flux ratio over a length of 11″. In the region

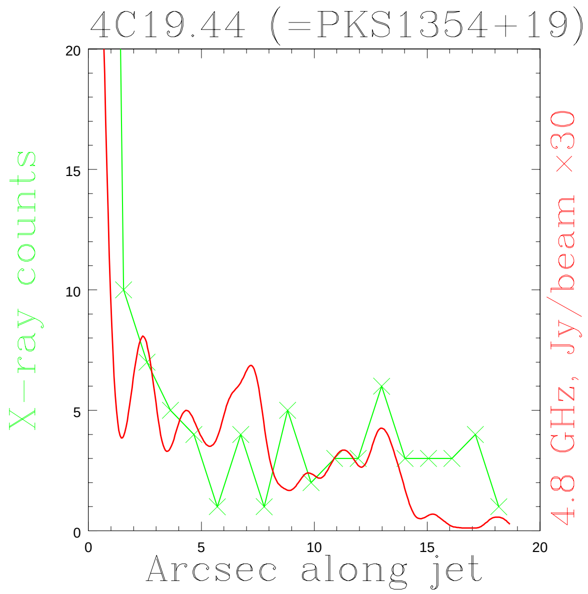

Fig. 9. Comparison of the X-ray (crosses) and 4.8 GHz radio (continuous line) profiles of the jet in 1354+195=4C19.44. The X-ray data is counts per bin, while the radio is flux density per beam times 30.

around 13″ to 15″ along the jet, this source may also be showing the behavior predicted by the IC/CMB mechanism. We see both the X-ray and radio increasing around 13″ but then the radio flux drops in the 15″ to 17″ region while the X-ray emission remains steady, as qualitatively expected if the X-rays are emitted by lower energy electrons via IC/CMB. However, cases of the opposite behavior have been cited (Stawarz et al. 2004), so this kind of argument probably cannot be used to diagnose the emission mechanism until we have a better understanding of the overall jet structure and dynamics.

The right hand panels of Figures 7 and 8 plot the radiated energy, νf_ν for the X-ray (crosses), 8.64 GHz (circles) and 4.8 GHz (triangles, PKS 1202-262) bands in absolute physical units, Jy-Hz. This shows that the X-rays are dominating the radiated emission of the jets, at least in those regions where X-rays are detected.

4. PHYSICAL PROPERTIES OF THE JETS

As discussed in Section 2.2 if the X-rays are produced by IC/CMB, then we can exploit the minimum energy assumptions typically used to interpret radio observations in order to estimate both the average magnetic field strength in the jet and the Doppler factor of the jet. This calculation was graphically illustrated in Figure 4, a diagram first used by Tavecchio et al. (2000). Figure 10 shows the results for

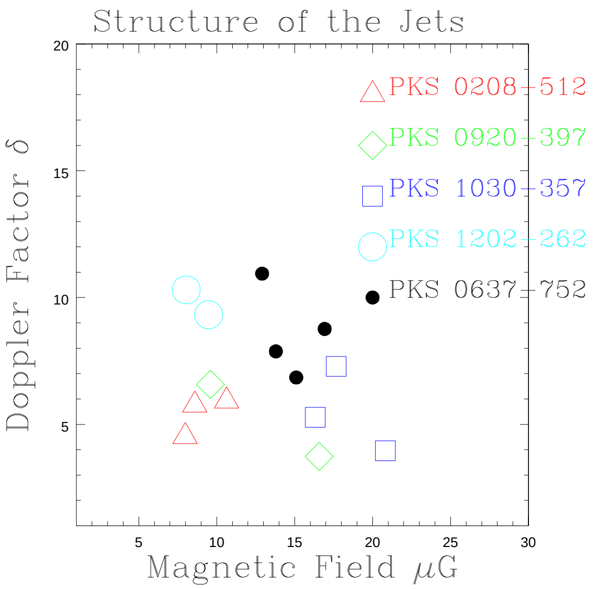

Fig. 10. Doppler factors and magnetic field strengths deduced for distinct spatial regions of several jets: triangles, PKS 0208-512; diamonds, PKS 0920-397; squares, PKS 1030-357; circles, PKS 1202-262; solid dots, PKS 0637-752. The results assume the radio arises from electrons in near-equipartition with the magnetic field in which they radiate synchrotron emission, and that the X-rays arise from IC/CMB.

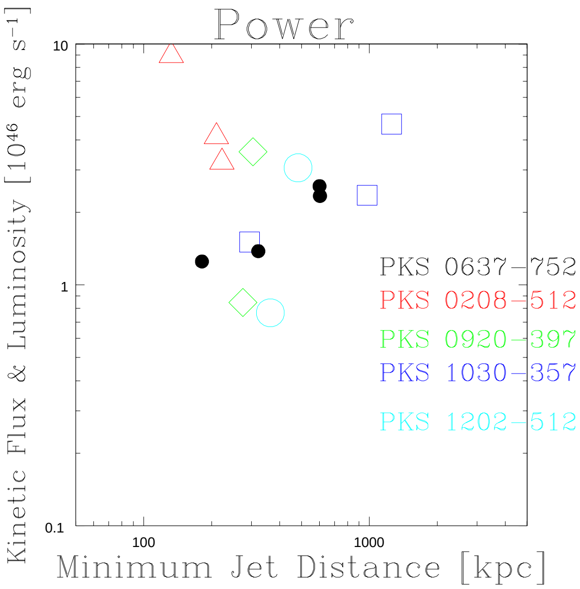

Fig. 11. Kinetic flux through distinct regions of five jets, vs. the deprojected minimum distance of that region from the quasar. Key to objects is the same as in Fig. 10.

spatially distinct regions of four jets from the Marshall et al. (2005) survey, and for PKS 0637-752 from Schwartz (2004). For these we see a range of rest frame magnetic fields B = 5 to 25 μG, and Doppler factors δ = 3 to 12.

Table 1 gives these and other quantities for spatially resolved regions of four jets as derived by Schwartz et al. (2006) from our model assumptions. The first column gives the PKS B name of the quasar, and the designation of the specific region along the jet. A question mark after the region designation indicates less than 10 X-ray photons, so that the identification with the radio emission is not certain. The second column is the redshift of the quasar. The next columns give the values of B and δ derived from the X-ray and radio data. Column 5 gives the Lorentz factor of the low energy cutoff of the electron spectrum, consistent with our assumption that the observed radio spectrum extends down to only 10^6 Hz. This is obviously quite arbitrary; see Worrall & Birkinshaw (2005) for a formalism assuming a $\gamma_{\rm min}$ intrinsic to the source. From our value of $\gamma_{\rm min}$ we calculate the total electron volume density by equating the particle energy density to that in the magnetic field:

$(1+k_1)\int_{\gamma_{min}}^{\gamma_{max}} n_0 m_e c^2 \gamma^{1-m} d\gamma \approx B^2/(8\pi)$, where k_1 is the ratio of proton to electron energy and m is the spectral index of the electron distribution. We have assumed k_1=1 and m=2.4.

For any fixed Doppler factor, the jet cannot be at an angle greater than $\arccos[(\sqrt{(\delta^2-1)})/\delta]$ from our line of sight, and which corresponds to the case $\Gamma = \delta$ which we have assumed. This maximum angle is given in column 7, and gives a minimum 3-dimension distance from the quasar of $x/\sin(\theta_{\rm max})$ where x is the apparent distance in the plane of the sky at the given redshift.

Among the most important information added by the X-ray observations is the ability to estimate the Doppler factor, and hence to calculate the kinetic energy flux carried by the jet. This is still dependent of course on the validity of near-equipartition conditions, uniformity of particle densities and magnetic field strength, and assumed values for several parameters which are not observed. The correct expression, as discussed by Bicknell (1994), considers that the kinetic energy density is the enthalpy density $w=\epsilon+\rho_0 c^2+p$, where ϵ is the internal energy density, ρ_0 the rest mass density, and p is the pressure. For $\beta \approx 1$, the jet power, $P_{\rm jet}= A\ \Gamma^2\ (w-\rho_0\ c^2/\Gamma)$, where A is the cross sectional area. This quantity is tabulated in column 9 of Table 1. The kinetic fluxes would be about 3 times lower if k_1=0, and about 10 times larger if k_1=10, instead of k_1=1 as we have assumed.

TABLE 1

PROPERTIES OF THE X-RAY JETS

PKS Name (region)	Redshift[a]	B [μG]	δ	γ_{min}[b]	n_e 10^{-8} cm^{-3}	θ_{max}[c] [deg]	Minimum Length[d]	Kinetic Flux[e]	Radiative Efficiency[f]
0208-512	0.999	...	...	...	...	...	...	...	...
(R1)		10.9	7.3	77	1.1	7.8	156	9.5	0.3
(R2)		13.5	7.5	69	1.8	7.7	262	3.6	1.2
(R3)?		10.1	5.7	91	0.78	10.1	246	3.8	0.5
0920-397	0.591	...	...	...	...	...	...	...	...
(R1)		12.1	8.3	61	1.7	6.9	322	1.0	1.0
(R2)?		20.8	4.7	62	4.8	12.3	356	3.8	0.2
1030-357	1.455	...	...	...	...	...	...	...	...
(R1)?		27.1	5.2	64	7.9	11.1	362	1.7	4.1
(R2)		22.3	9.2	53	6.5	6.2	1155	3.4	1.8
(R3)		20.9	6.7	65	4.7	8.6	1484	5.5	3.0
1202-262	0.789	...	...	...	...	...	...	...	...
(R1)		10.6	13.5	55	1.4	4.2	443	0.9	2.2
(R2)		12.0	11.8	55	1.8	4.9	568	4.0	0.6

[a]From the NED database, operated by JPL for NASA

[b]Calculated from B so that electrons of γ_{min} give 1 MHz synchrotron emission

[c]Calculated assuming bulk Lorentz factor Γ equals Doppler factor δ

[d]Minimum distance from quasar, deprojected by $1/\sin(\theta_{max})$, in kpc

[e]Kinetic power of jet, 10^{46} erg s^{-1}

[f]De-beamed luminosity divided by kinetic flux, in 10^{-4}

In Figure 11 we plot the kinetic power flowing through any region, as a function of the (minimum) distance of that region from the quasar. Considering possible factor of two uncertainties in B or δ due to the model assumptions, the results are probably consistent with a constant power flowing the length of the jet. This is the reasonable expectation, as there is no source of energy at such distance from the quasar. The radiative efficiency of the jet is extremely low, indicated in column 10 of Table 1, so there is also no evident energy loss from the jet prior to a terminal hotspot. However, at such relatively large redshifts and short exposure times we might not be able to detect an intercluster medium with which the jet interacts. If the data required an apparent increase in power with increasing distance from the quasar, we could invoke deceleration of the outer jet (which might force an alternate to the IC/CMB X-ray emission mechanism) or consider, for example, different proton to electron energy ratios along the jet, in order to model a constant kinetic power along the jet. Alternately, the high power region could indicate an epoch of higher than average activity from the quasar.

We compare these fluxes with the quasar bolometric radiative luminosity, estimated by fitting the radio loud template of Elvis et al. (1994) to the optical magnitude from the NED database, assuming isotropic emission, and integrating over all wavelengths. We obtain 9, 0.35, 1, and 0.6 $\times$ 10^{46} ergs s^{-1}, respectively, for PKS 0208, PKS 0920, PKS 1030, and PKS 1202. Those are all lower, or at most equal, to the kinetic power being transported out by the jet.

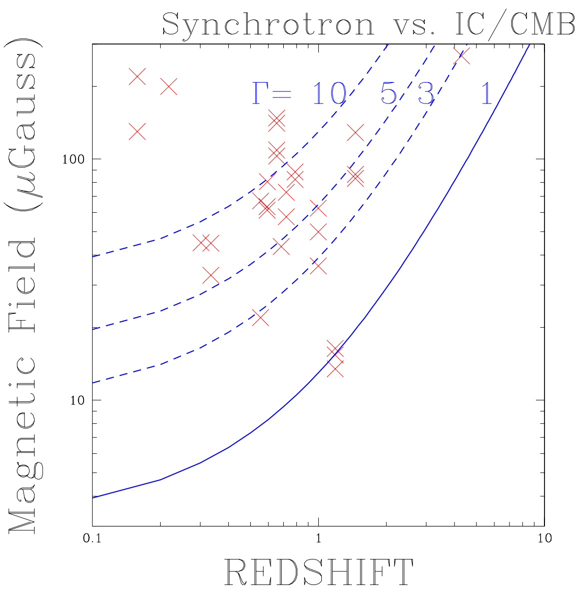

Fig. 12. The locus of magnetic field strengths for which we have equal magnetic energy density and CMB energy density at the given redshift. The solid line shows the case where jets are all non-relativistic, while the dashed lines show various Lorentz factors in the range deduced by *Chandra* observations of quasar jets. The crosses give magnetic fields calculated to produce radio emission via the minimum energy formalism but ignoring the possibility of relativistic motion.

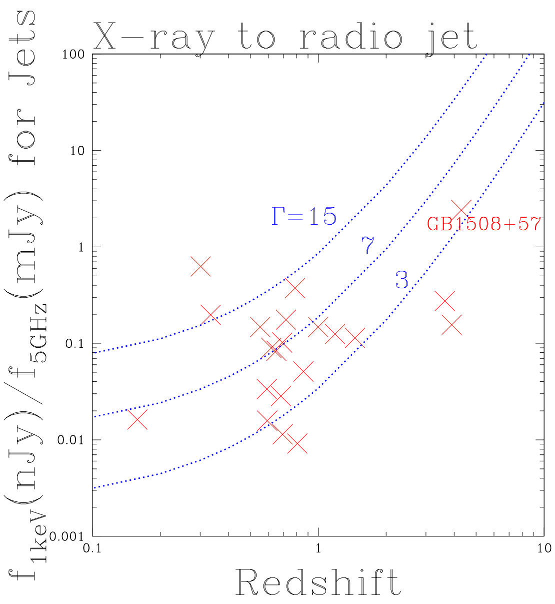

Fig. 13. The crosses plot the measured ratios of integrated X-ray to radio fluxes from jets measured by *Chandra*, vs. their redshift. The dotted lines show how these ratios would be expected to change if the identical jet were at different redshifts, and for different bulk Lorentz factors of 3, 7, 15. The dotted curves are normalized to the observation of PKS 0637-752.

5. JETS AT LARGE REDSHIFT

Is inverse Compton scattering from the cosmic microwave background the source of the X-ray emission from relativistic jets? We believe this is the best assumption based on observations to date; however, it is extremely important to verify if this is true. If we are already observing IC/CMB X-rays, then because the CMB energy density increases as $(1+z)^4$, exactly compensating for the $(1+z)^{-4}$ cosmological diminution of surface brightness, objects intrinsically identical to any of the jets which we have studied will be easily detected at however large a redshift they might exist (Schwartz 2002). In this case, even the non-detection of objects will give us information on the evolutionary history of massive black hole formation and activity in the early universe.

Figure 12 shows that IC/CMB is almost certain to be operating for at least some objects. The ratio of synchrotron to IC/CMB energy loss for electrons is determined by the ratio of the target energy densities, $B^2/8\pi$ and $\rho_{CMB}=\Gamma^2(1+z)^4\rho_0$ where $\rho_0 = 4.19 \times 10^{-13}$ ergs cm^{-3} is the local CMB energy density. The solid line shows equality in case of non-relativistic motion, Γ=1. For magnetic fields below that line, IC/CMB would dominate, while synchrotron radiation would dominate when the magnetic field at any redshift were above the line. The dashed lines show how progressively larger magnetic fields are required for synchrotron radiation to dominate the X-ray emission when the jet is in relativistic motion with the Γ value as labeled. The crosses in Figure 12 show the magnetic fields calculated assuming only minimum energy, and no relativistic motion. In order to avoid IC/CMB X-rays, we must not have any jets with bulk Lorentz factors greater than about 3, or else all the jets must have magnetic fields greatly in excess of the minimum energy or near-equipartition value. In fact, when we model the X-ray emission as IC/CMB, we deduce that magnetic fields in the jets are typically 5 to 30 μG, much weaker than the values plotted assuming no relativistic motion.

Even in the case where Γ is no greater than 3, whatever small fraction of IC/CMB X-rays are being produced at the current redshift will be manifested as a constant surface brightness source to larger redshift, and will eventually dominate the synchrotron emission. For example, if we consider the jet at redshift about 0.3 with magnetic field 40 μG, it must be emitting at least 10% of its X-ray flux via IC/CMB if Γ=3 (since a magnetic field only 3 times weaker would place it below the corresponding dashed line). Because our 5 ks observations are photon limited, a modest *Chandra* observation of 50 ks would detect such an object at any redshift.

Do observations support the prediction that the X-ray jets become predominant at larger redshifts? The systematic surveys carried out by Marshall et al. (2005) and Sambruna et al. (2004) have observed objects clustered broadly around a redshift of about 1. These objects show a significant dispersion in their X-ray to radio flux ratio (Figure 13), no doubt due to both an intrinsic dispersion and to differences in their bulk Lorentz factors and the angles of their jets to our line of sight. At smaller redshifts we see just a few special objects in our vicinity, e.g., Cen A, M87, and 3C 273, while at larger redshifts the jet detections are of just a few serendipitous objects (Siemiginowska et al. 2003; Cheung, Wardle, & Lee 2004). Those few objects at redshifts above 3 in Figure 13 certainly do not show the dramatic increase which we might expect. However, this is easily explained since we might expect the objects with lowest Lorentz and Doppler factors to be most numerous, and these may be undetectable in X-rays *unless* at high redshift. In fact, GB 1508+57 at z=4.3 has the highest f_X/f_{5GHZ} ratio, which is more than an order of magnitude greater than the median for the survey objects. Therefore, no conclusion on the validity of the IC/CMB mechanism can yet be drawn from this diagram.

6. SUMMARY

The systematic study of X-ray jets has only become possible with the superb angular resolution of the *Chandra* X-ray Observatory. The surveys to date have made primarily short duration observations, but show that X-ray emission is a common feature of relativistic quasar jets, and typically dominates the radiative power of the jet. If the emission is due to inverse Compton scattering on the cosmic microwave background, then in conjunction with the usual radio astronomy models of minimum synchrotron emission we can estimate the effective Doppler factors, the rest frame magnetic field strength, the low energy cutoff of the relativistic electron spectrum, and the kinetic flux, all in numerous spatially resolved regions extending up to 1 Mpc from the parent quasar. By modeling the run of these parameters along a jet, we can expect to learn about acceleration sites, the deceleration of the bulk motion of the jet, and perhaps the proton content.

From the direct estimates of kinetic power carried by powerful quasar jets, we know that if such systems occurred within rich clusters of galaxies that their jets would provide more than enough energy to power the radio cavities discovered in clusters (Birzan 2004) and thus stop the cooling flows. And since the quasar/jet phenomenon appears to involve only massive black holes supplied by gas deep within a galaxy, it would be very hard to understand why such jets would *not* also occur in clusters.

We saw that in many cases the kinetic power is comparable to or in excess of the quasar radiative power. Since a jet is highly anisotropic, it is not subject to an Eddington limit, and might be providing a clue that quasars can accrete mass much in excess of the Eddington limit with the corollary that massive black holes could grow very quickly.

The most significant implication is due to the fact that a given IC/CMB jet would maintain a constant surface brightness no matter what its redshift. X-ray detection of such objects might reveal some of the earliest activity in the universe. Some such objects must already have been detected by *ROSAT* surveys, but would be anonymous, unidentified sources. Bright *ROSAT, ASCA*, or *Einstein* quasar identifications could have substantial jet components, which those observatories would not be able to resolve spatially from the quasar core.

The IC/CMB mechanism gives clear predictions for finding larger X-ray to radio flux ratios in objects at large redshift, and for finding γ-ray jets in quasars just about at the level of *GLAST* sensitivity. Precise measurement of the X-ray spectra of the jets should give slopes equal to, or flatter than, the GHz radio slope, since the X-rays are emitted by electrons with lower energies. Longer *Chandra* observations of the known X-ray jets, and systematic surveys of kpc-scale radio jets at large redshifts, will test these predictions.

This work was supported by NASA contract NAS8-39073 to the *Chandra* X-ray Center, and NASA/CXO grants GO2-3151C, GO3-4120X, and GO4-5108X to SAO. The work discussed here has benefited from contributions and discussions with collaborators in our jet survey: H.L. Marshall, J.M. Gelbord, E.S. Perlman, M. Georganopoulos, M. Birkinshaw, D.M. Worrall, J.E.J. Lovell, D.L. Jauncey, L. Godfrey, G.V. Bicknell, D.W. Murphy, and S. Jester This research has made use of NASA's Astrophysics Data System Bibliographic Services, and the NASA/IPAC Extragalactic Database which is operated by the Jet Propulsion Laboratory, California Institute of Technology, under contract with the National Aeronautics and Space Administration.

REFERENCES

Begelman, M. C., Blandford, R. D., & Rees, M. J. 1984, Reviews of Modern Physics, 56, 255
Bicknell, G. V. 1994, ApJ, 422, 542
Birzan, L., Rafferty, D. A., McNamara, B. R., Wise, M. W., Nulsen, P. E. J. 2004, ApJ, 607, 800
Celotti, A., Ghisellini, G., & Chiaberge, M. 2001, MNRAS, 321, L1
Cheung, C. C., Wardle, J. F. C., & Lee, N. P. 2004, in *Proceedings of the 22nd Texas Symposium, Palo Alto, 2004* edited by P. Chen, eConf C041213:1613
Dermer, C. D. & Schlickeiser, R. 1994, ApJS, 90, 945
Elvis, M. et al. 1994, ApJS, 95, 1
Fabian, A. C. 1994, ARA&A, 32, 277
Felten, J. E. & Morrison, P. 1966, ApJ, 146, 686
Harris, D. E., Biretta, J. A., Junor, W., Perlman, E. S., Sparks, W. B., Wilson, A. S. 2003, ApJ, 586, L41
Lovell, J. 1997, Ph.D. Thesis, U. of Tasmania
Marshall, H. L., et al. 2001, ApJ, 549, L167
Marshall, H. L., et al. 2005, ApJS, 156, 13
Moffet, A. T. 1975, in Galaxies and the Universe, ed. A. Sandage, M. Sandage, J. Kristian, (Chicago: University of Chicago Press), 211
Murphy, D.W., Browne, I.W.A., & Perley, R.A. 1993, MNRAS, 264, 298
Perlman, E. S., et al., 2004, AAS HEAD meeting 8, 04.19
Sambruna, R. M., Maraschi, L., Tavecchio, F., Urry, C. M., Cheung, C. C., Chartas, G., Scarpa, R., & Gambill, J. K. 2002, ApJ, 571, 206
Sambruna, R. M., Gambill, J.K., Maraschi, L., Tavecchio, F., Cerutti, R., Cheung, C. C., Urry, C. M., & Chartas, G., 2004, ApJ, 608, 698
Schreier, E. J., Burns, J. O., & Feigelson, E. D. 1981 ApJ, 251, 523
Schwartz, D. A., et al. 2000,ApJ, 540, L69
Schwartz, D. A., et al. 2001, in X-ray Astronomy 2000, ASP Conference Proceeding Vol. 234. Edited by Riccardo Giacconi, Salvatore Serio, & Luigi Stella. (San Francisco: Astronomical Society of the Pacific) 493
Schwartz, D. A. 2002, ApJ, 569, L23
Schwartz, D. A. 2004, in *Proceedings of the 22nd Texas Symposium, Palo Alto, 2004* edited by P. Chen, eConf C041213:0027
Schwartz, D. A. et al. 2006, ApJ, in press
Siemiginowska, A. et al. 2003, ApJ, 598, L15
Stawarz, Ł., Sikora, M., Ostrowski, M., & Begelman, M. C. 2004, ApJ, 608, 95
Tavecchio, F., Maraschi,L., Sambruna, R. M., & Urry, C. M. 2000, ApJ, 544, L23
Worrall, D. M., Birkinshaw, M., & Hardcastle, M. J. 2001, MNRAS, 326, L7
Worrall, D. M., & Birkinshaw, M. 2005, in "Physics of Active Galactic Nuclei at all Scales," D. Alloin, R. Johnson, P. Lira, eds., (Springer Verlag, Lecture Notes in Physics series), also astro-ph/0410297

Daniel A. Schwartz: Smithsonian Astrophysical Observatory, 60 Garden Street, Cambridge, MA 02138, USA (das@cfa.harvard.edu).